J|A|C|S
ARTICLES
Published on Web 06/01/2006

Divergent Growth of Coordination Dendrimers on Surfaces

Meni Wanunu,[†] Alexander Vaskevich,[†] Abraham Shanzer,[‡] and Israel Rubinstein*[,†]

Contribution from the Department of Materials and Interfaces and Department of Organic Chemistry, Weizmann Institute of Science, Rehovot 76100, Israel

Received March 14, 2006; E-mail: israel.rubinstein@weizmann.ac.il

Abstract: Divergent growth of surface-initiated dendritic nanostructures on gold surfaces in a highly controlled, stepwise manner is demonstrated, using metal−organic coordination as the binding motif. The repeat unit for dendrimer growth was a branched, C_3-symmetrical ligand building block bearing three bis-hydroxamate groups. The surface initiation sites for dendrimer growth were obtained by the formation of a mixed monolayer comprising isolated bis-hydroxamate disulfide anchor ligands and octanethiol (OT) at very low anchor/OT ratios. Following functionalization of the surface with spaced anchors, alternate immersion in solutions of Zr^{4+} ions and the branched ligand afforded surface-confined dendrimers of increasing generation, where the number of generations is conveniently controlled by the number of coordination binding sequences. The heights of different generation dendrimers are in excellent agreement with values predicted by molecular models, as well as with thicknesses of branched multilayers prepared by the same procedure on full anchor monolayers. At higher generation numbers, gradual dendrimer overlap and coalescence are observed, eventually resulting in a continuous overlayer and a transition from 3D to 1D growth. A mechanism for the development of dendritic coordination nanostructures on surfaces is discussed.

Introduction

In recent years, there has been increasing interest in the development of new techniques for patterning surfaces with nanoscale materials.[1−6] This trend, largely a result of recent efforts aimed at miniaturization of components and devices, received a substantial boost with the recent development of advanced characterization tools, which currently enable routine investigations on the nanometer scale and down to single molecule resolution. While there are different strategies for nanoscale patterning on surfaces, achieving simultaneous control of the position and dimensions of nano-objects is a highly demanding task. Although the ultimate goals of surface nanopatterning are rather generally defined, several parameters have been identified as immediate objectives, such as control over the distance between nano-objects, their density, size, and function. It is anticipated that manipulation of these parameters would enable achievement of novel surface structures and functions, and this topic is therefore a thriving area of research.

Control over the size distribution of nanoscale objects is no trivial task; although the average size of nanoparticles or polymers can usually be controlled, the size distribution tends to broaden as smaller objects are synthesized. Since nanoscale materials frequently exhibit size-dependent properties, achieving size uniformity is highly desirable. One way to minimize polydispersity is by limiting the growth of the object size using specialized stepwise reactions. In solution, such control has been realized with dendrimers, which are branched, treelike molecules obtained by a repetitive sequence of activation/reaction steps.[7] With features such as precise size and mass, multiple peripheral functional groups, and (possibly) a functional interior structure, dendrimers are ideal building blocks for nanoscale surface patterning.[8] Indeed, surface immobilized dendrimers and other dendritic structures[9] have attracted much attention in the past decade.[10−23] The sensitivity of surface-immobilized dendrimers toward volatile organic compounds (VOCs) has been studied.[24−26]

[†] Department of Materials and Interfaces.
[‡] Department of Organic Chemistry.

(1) Hammond, P. T. *Adv. Mater.* **2004**, *16*, 1271−1293.
(2) Gates, B. D.; Xu, Q. B.; Love, J. C.; Wolfe, D. B.; Whitesides, G. M. *Annu. Rev. Mater. Res.* **2004**, *34*, 339−372.
(3) Smith, R. K.; Lewis, P. A.; Weiss, P. S. *Prog. Surf. Sci.* **2004**, *75*, 1−68.
(4) Lussi, J. W.; Michel, R.; Reviakine, I.; Falconnet, D.; Goessl, A.; Csucs, G.; Hubbell, J. A.; Textor, M. *Prog. Surf. Sci.* **2004**, *76*, 55−69.
(5) Segalman, R. A. *Mater. Sci. Eng., R:* **2005**, *48*, 191−226.
(6) Gitsov, I.; Lin, C. *Curr. Org. Chem.* **2005**, *9*, 1025−1051.
(7) Newkome, G. R.; Moorefield, C. N.; Vogtle, F. *Dendrimers and Dendrons*; VCH: Weinheim, 2002.
(8) Tomalia, D. A. *Prog. Polym. Sci.* **2005**, *30*, 294−324.
(9) The term dendritic structures is used here to describe irregularly branched systems, as opposed to the regular branching exhibited in dendrimers.
(10) Watanabe, S.; Regen, S. L. *J. Am. Chem. Soc.* **1994**, *116*, 8855−8856.
(11) Alonso, B.; Moran, M.; Casado, C. M.; Lobete, F.; Losada, J.; Cuadrado, I. *Chem. Mater.* **1995**, *7*, 1440−1442.
(12) Liu, Y. L.; Bruening, M. L.; Bergbreiter, D. E.; Crooks, R. M. *Angew. Chem., Int. Ed. Engl.* **1997**, *36*, 2114−2116.
(13) Tsukruk, V. V. *Adv. Mater.* **1998**, *10*, 253.
(14) Huck, W. T. S.; van Veggel, F.; Sheiko, S. S.; Moller, M.; Reinhoudt, D. N. *J. Phys. Org. Chem.* **1998**, *11*, 540−545.
(15) Lackowski, W. M.; Franchina, J. G.; Bergbreiter, D. E.; Crooks, R. M. *Adv. Mater.* **1999**, *11*, 1368−1371.
(16) Huisman, B. H.; Schonherr, H.; Huck, W. T. S.; Friggeri, A.; van Manen, H. J.; Menozzi, E.; Vancso, G. J.; van Veggel, F.; Reinhoudt, D. N. *Angew. Chem., Int. Ed.* **1999**, *38*, 2248−2251.
(17) Rahman, K. M. A.; Durning, C. J.; Turro, N. J.; Tomalia, D. A. *Langmuir* **2000**, *16*, 10154−10160.
(18) Friggeri, A.; van Manen, H. J.; Auletta, T.; Li, X. M.; Zapotoczny, S.; Schonherr, H.; Vancso, G. J.; Huskens, J.; van Veggel, F.; Reinhoudt, D. N. *J. Am. Chem. Soc.* **2001**, *123*, 6388−6395.
(19) Emmrich, E.; Franzka, S.; Schmid, G. *Nano Lett.* **2002**, *2*, 1239−1242.
(20) Li, C.; Mitamura, K.; Imae, T. *Macromolecules* **2003**, *36*, 9957−9965.
(21) Kim, B. Y.; Bruening, M. L. *Langmuir* **2003**, *19*, 94−99.

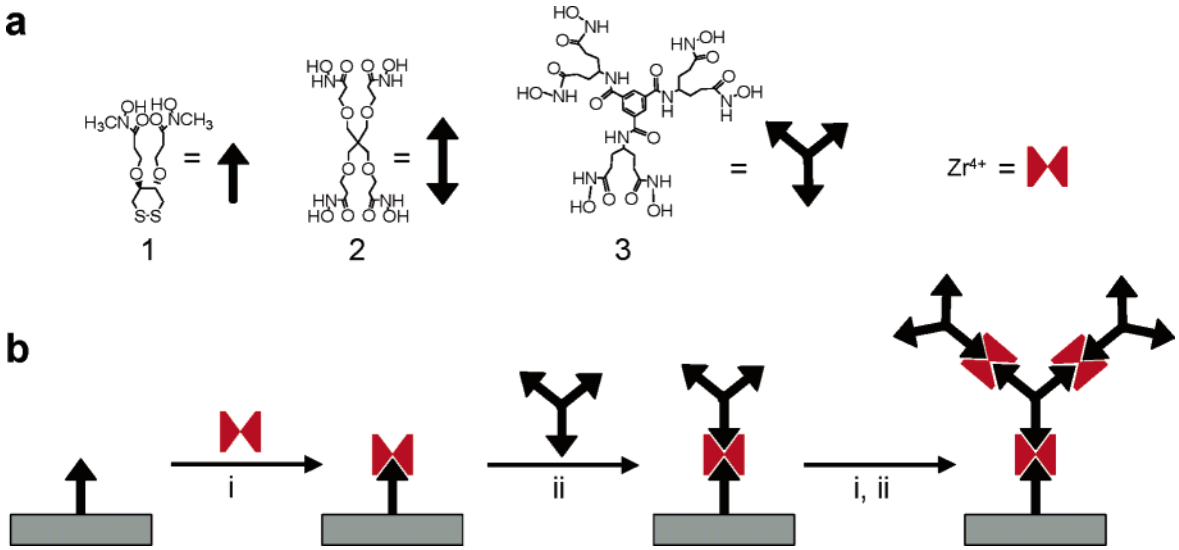

Figure 1. (a) Schematic presentation of the ligand anchor **1**, "linear" building block **2**, branched building block **3**, and the metal ion. (b) The general scheme for the construction of coordination dendrimers of **3**, showing two generations of **3** grown from an isolated binding site of **1**.

Surface dendrimer films have been used as adhesion promoters for evaporated metallic films[27] and as anchors for electroless pattern metallization.[28] Adsorption of dendritic wedges on surfaces was reported to provide lateral spacing between biotin moieties attached to the exposed core of the dendrite, thereby enabling unhindered access for streptavidin binding, showing utility for biochip applications.[29] Ferrocene-modified dendrimers were bound to β-cyclodextrin-modified surfaces through multiple binding sites, forming stable and reversible assemblies.[30] Amine-terminated dendrimer assemblies on surfaces were shown to be highly reactive substrates for protein immobilization, useful for various biosensor applications.[31,32]

The above reports concern binding of preformed dendrimers or dendritic wedges to surfaces. Stepwise construction of dendritic structures on surfaces has also been studied by several groups.[24,33−37] The general scheme involves exposure of a surface derivatized with a known functional group to a step-by-step reaction with a branched molecule. Each repeated sequence of reactions (generation) increases the branching and, hence, the number of surface functional groups. Such controlled growth is reminiscent of the common layer-by-layer (LbL) assembly of multilayers on surfaces, where growth is initiated from a full layer of active molecules and each step adds a thickness increment corresponding to one building block.[38] Advantages of branched growth initiated at specific points on the surface include control over the size of the features, the density of functional groups, and the surface structure. Notably, the use of surface reactions to grow dendritic structures is especially convenient, as it may be carried out with relatively simple molecules and straightforward immersion/rinse cycles; this is in contrast with solution synthesis of dendrimers, which must involve tedious deprotection/reaction steps and repeated purifications, thereby increasing the complication and cost. These complex steps are avoided in the surface dendrimer growth scheme, by the inherent isolation and confinement of the growing dendritic structures. The stepwise approach for dendritic growth is therefore highly attractive for surface patterning with nanoscale objects of controlled dimensions and chemical functionalities.

We recently demonstrated LbL growth of branched coordination multilayers on gold surfaces, based on the C_3-symmetrical (hexahydroxamate) ligand building block **3** (Figure 1). Binding between the repeat organic layers was based on metal−organic coordination of the bis-hydroxamate groups with tetravalent metal ions such as Zr^{4+}.[39] Briefly, the surface was first primed with a self-assembled monolayer (SAM) of the disulfide bishydroxamate ligand **1** (Figure 1), similar to schemes used by us previously for the construction of coordination monolayers and multilayers.[40−43] This was followed by alternate binding of single layers of the branched building block **3** and metal ions,

(22) Kleijn, J. M.; Barten, D.; Stuart, M. A. C. *Langmuir* **2004**, *20*, 9703−9713.
(23) Ostmark, E.; Macakova, L.; Auletta, T.; Malkoch, M.; Malmstrom, E.; Blomberg, E. *Langmuir* **2005**, *21*, 4512−4519.
(24) Wells, M.; Crooks, R. M. *J. Am. Chem. Soc.* **1996**, *118*, 3988−3989.
(25) Tokuhisa, H.; Crooks, R. M. *Langmuir* **1997**, *13*, 5608−5612.
(26) Zhang, H.; Grim, P. C. M.; Foubert, P.; Vosch, T.; Vanoppen, P.; Wiesler, U. M.; Berresheim, A. J.; Mullen, K.; De Schryver, F. C. *Langmuir* **2000**, *16*, 9009−9014.
(27) Street, S. C.; Rar, A.; Zhou, J. N.; Liu, W. J.; Barnard, J. A. *Chem. Mater.* **2001**, *13*, 3669−3677.
(28) Bittner, A. M.; Wu, X. C.; Kern, K. *Adv. Funct. Mater.* **2002**, *12*, 432−436.
(29) Choi, Y. S.; Yoon, C. W.; Lee, H. D.; Park, M.; Park, J. W. *Chem. Commun.* **2004**, 1316−1317.
(30) Nijhuis, C. A.; Huskens, J.; Reinhoudt, D. N. *J. Am. Chem. Soc.* **2004**, *126*, 12266−12267.
(31) Pathak, S.; Singh, A. K.; McElhanon, J. R.; Dentinger, P. M. *Langmuir* **2004**, *20*, 6075−6079.
(32) Yang, M.; Tsang, E. M. W.; Wang, Y. A.; Peng, X. G.; Yu, H. Z. *Langmuir* **2005**, *21*, 1858−1865.
(33) Zhang, L.; Bo, Z. S.; Zhao, B.; Wu, Y. Q.; Zhang, X.; Shen, J. C. *Thin Solid Films* **1998**, *329*, 221−223.
(34) Kim, H. J.; Moon, J. H.; Park, J. W. *J. Colloid Interface Sci.* **2000**, *227*, 247−249.
(35) van Manen, H. J.; Auletta, T.; Dordi, B.; Schonherr, H.; Vancso, G. J.; van Veggel, F.; Reinhoudt, D. N. *Adv. Funct. Mater.* **2002**, *12*, 811−818.
(36) Seckin, T.; Gultek, A. *J. Appl. Polym. Sci.* **2003**, *90*, 3905−3911.
(37) Wu, X. Z.; Liu, P.; Pu, Q. S.; Sun, Q. Y.; Su, Z. X. *Talanta* **2004**, *62*, 918−923.
(38) Ulman, A. *An Introduction to Ultrathin Organic Films*; Academic Press: Boston, 1991.
(39) Wanunu, M.; Vaskevich, A.; Cohen, S. R.; Cohen, H.; Arad-Yellin, R.; Shanzer, A.; Rubinstein, I. *J. Am. Chem. Soc.* **2005**, *127*, 17877−17887.
(40) Hatzor, A.; Moav, T.; Cohen, H.; Matlis, S.; Libman, J.; Vaskevich, A.; Shanzer, A.; Rubinstein, I. *J. Am. Chem. Soc.* **1998**, *120*, 13469−13477.
(41) Moav, T.; Hatzor, A.; Cohen, H.; Libman, J.; Rubinstein, I.; Shanzer, A. *Chem.—Eur. J.* **1998**, *4*, 502−507.
(42) Hatzor, A.; van der Boom-Moav, T.; Yochelis, S.; Vaskevich, A.; Shanzer, A.; Rubinstein, I. *Langmuir* **2000**, *16*, 4420−4423.
(43) Doron-Mor, I.; Cohen, H.; Cohen, S. R.; Popovitz-Biro, R.; Shanzer, A.; Vaskevich, A.; Rubinstein, I. *Langmuir* **2004**, *20*, 10727−10733.

to afford coordination multilayers. The branched multilayers thus produced showed highly regular growth, no evolution of surface roughness, and lateral cross-linking in the layers, induced by the excess available ligand groups.

Despite the great interest in combining dendritic growth on surfaces with coordination chemistry, the only case known to us where stepwise growth of surface dendrimers using coordination chemistry was described is the work of Reinhoudt and coworkers, who used SCS/Pd^{2+}-to-pyridine chemistry for the self-assembly of Frechet-type dendrons.[35] In the present work we describe a facile stepwise formation of coordination metallodendritic structures prepared by the assembly of centrosymmetric ligand building blocks on highly dilute ligand-functionalized gold surfaces. Dendritic growth using both linear (**2**, Figure 1) and branched (**3**, Figure 1) building blocks on gold was investigated, showing coalescence of adjacent dendrimers and remarkably efficient space-filling, resulting in a transition of the film structure from isolated dendrimers to full layers with the increase in the number of generations. The systems were investigated by ellipsometry, contact-angle (CA) measurements, X-ray photoelectron spectroscopy (XPS), and atomic force microscopy (AFM).

Experimental Section

Chemicals and Materials. The syntheses of the hydroxamate ligands **1**−**3** are described elsewhere.[39,41] $Zr(acac)_4$ (99%, Strem) was used as received. Water was purified by ion-exchange columns followed by double distillation. 1-Octanethiol (OT) (98.5%, Aldrich) was vacuum distilled and stored under N_2. Chloroform (AR, Biolab) was passed through a column of activated basic alumina prior to use. Ethanol (AR, Baker) and methanol (AR, Mallinckrodt) were used as received.

Substrate Preparation. The gold substrates used in all experiments were 100 nm gold evaporated on aminosilanized Si(111) wafers and annealed in air (220 °C, 20 h), as described elsewhere.[44] All glassware was cleaned with boiling piranha solution followed by copious rinsing with water. (*Caution:* Piranha solution reacts violently with organic materials and should be handled with extreme care.) Samples were dried using 0.2 μm PTFE-filtered household N_2 (>99%, from liquid N_2).

Self-Assembly. (a) Improved OT SAMs: The preparation of improved OT SAMs is described in detail elsewhere.[45] Briefly, the procedure includes the following steps: (1) A clean gold substrate is immersed in a 10 mM ethanolic solution of OT for 1 h; (2) the substrate is subjected to a single voltammetric cycle in the gold oxidation/reduction regime in 0.1 M aq. H_2SO_4; (3) the substrate is immersed again in the OT solution overnight.

(b) Monolayers with varying density of anchor **1**: Dilute layers of anchor **1** in OT SAMs were prepared by immersion of an improved OT SAM into a 0.1 mM ethanolic solution of **1** for varying time periods, followed by rinsing with ethanol, 20 min immersion in stirred ethanol, and drying under N_2. Full SAMs of **1** were prepared by overnight immersion of a cleaned gold substrate in a 3 mM solution of **1** in 1:1 ethanol/chloroform, followed by rinsing with ethanol, 20 min immersion in stirred ethanol, and drying under N_2.[41]

(c) Coordination binding of Zr^{4+}, **2**, and **3**: Zr^{4+} ions were bound by 1 h immersion in a 1 mM ethanolic solution of $Zr(acac)_4$, followed by rinsing with ethanol, 20 min immersion in stirred ethanol, and drying under N_2.[43] Binding of the tetrahydroxamate ligand **2** was performed by overnight immersion in 3 mM ethanolic solution of **2**, followed by rinsing with ethanol, 20 min immersion in stirred ethanol, and drying under N_2.[43] The hexahydroxamate branched ligand **3** was bound similarly, using methanol as the solvent.[39] Ellipsometry, contact-angle (CA), and atomic force microscopy (AFM) measurements were performed after each ligand binding step.

Ellipsometry. Ellipsometric measurements were carried out with a Rudolph Research Auto-EL IV null ellipsometer, at an angle of incidence $\phi = 70°$ and a wavelength $\lambda = 632.8$ nm. The same four points were measured on each sample, with a typical precision of $\pm 0.1°$ in Δ and Ψ.

Contact-Angle (CA) Measurements. Advancing and receding CAs using pure water were measured with a computerized CA meter (KSV Instruments, Finland). Data collection and analysis were carried out using the manufacturer's CAM100 software. Average CAs of three measurements on each sample are reported.

Atomic Force Microscopy (AFM). All AFM images were obtained in air using a PicoSPM instrument (Molecular Imaging, USA), operating in the dynamic mode. Images were collected at scanning frequencies of 0.5−1 Hz. NSC-12 cantilever probes (Mikromasch, Estonia) with a resonant frequency of ca. 120 kHz and estimated tip radii < 10 nm were used.

X-ray Photoelectron Spectroscopy (XPS). XPS measurements were carried out with a Kratos AXIS-HS system, using a monochromatized Al (Kα) X-ray source ($h\upsilon = 1486.6$ eV). To minimize beam-induced damage, a low dose was maintained, using a relatively low beam flux (5 mA emission current at 15 keV) and medium energy resolution (pass energy of 80 eV).

Results and Discussion

The building blocks used in this work and the construction scheme are shown in Figure 1a, b, respectively. Molecules **1**−**3** are the anchor disulfide bishydroxamate, the "linear" tetrahydroxamate building block, and the branched hexahydroxamate building block, respectively. Figure 1b presents the experimental procedure for the preparation of branched dendritic structures using molecule **3**. Starting with a gold substrate functionalized with anchor **1**, the sequence (i, ii) is repeated *n* times to provide an *n*th generation surface-grown dendrimer. It is evident from the scheme in Figure 1b that uninterrupted growth of the dendritic structures requires an array of laterally spaced anchors on the surface, separated by inert regions. As a numerical example, using the estimated lateral dimensions of anchor molecule **1**, a monolayer coverage of ~0.1% is required to accommodate nonoverlapping 5-nm nanostructures (assuming regular spacing of **1** on the surface). Such low-density surface coverage values are difficult to achieve and quantify.

Our route to the preparation of SAMs with dilute anchors involved insertion of **1** into a preformed SAM of an inert alkanethiol, as previously used by other groups to obtain dilute functional SAMs.[18,46] Since anchor **1** is a relatively short molecule, we chose octanethiol (OT) as an inert alkanethiol of comparable length, to avoid masking of the bishydroxamate ion binding site of **1** by adjacent alkanethiols. It is assumed that anchor **1** is inserted at defects and pinholes in the OT monolayer; therefore, to attain a high dilution of **1** (i.e., large spacing) a high-quality SAM of OT is required. The latter was achieved using our method of electrochemical improvement of short-chain alkanethiol SAMs, as previously reported.[45] The improved OT SAM was immersed in a solution of anchor **1**, resulting in a gold surface covered with an inert OT SAM containing very low fractions of anchor **1**.[45]

(44) Wanunu, M.; Vaskevich, A.; Rubinstein, I. *J. Am. Chem. Soc.* **2004**, *126*, 5569−5576.
(45) Wanunu, M.; Vaskevich, A.; Rubinstein, I. *Israel Journal of Chemistry* **2005**, *45*, 337−344.
(46) Dunbar, T. D.; Cygan, M. T.; Bumm, L. A.; McCarty, G. S.; Burgin, T. P.; Reinerth, W. A.; Jones, L.; Jackiw, J. J.; Tour, J. M.; Weiss, P. S.; Allara, D. L. *J. Phys. Chem. B* **2000**, *104*, 4880−4893.

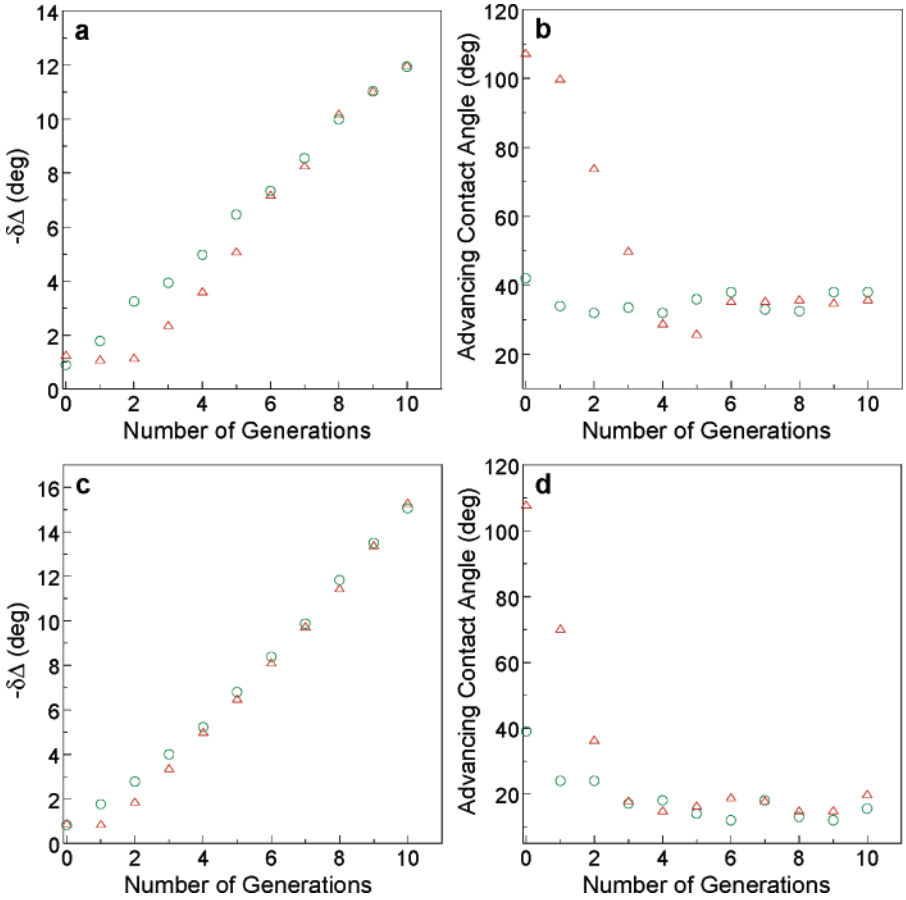

Figure 2. Changes in the ellipsometric Δ values (a) and advancing CAs (b) for the stepwise construction of 10 generations of Zr^{4+}/**2** on dilute (triangles) and full (circles) SAMs of anchor **1** (the 0th generation represents the dilute SAM of **1** in OT). Plots (c) and (d) show analogous stepwise construction of branched dendritic structures of Zr^{4+}/**3**. Dilute OT + **1** SAMs were prepared by 16 h immersion of an improved OT SAM in 0.1 mM ethanolic solution of **1**.

Figure 2 shows ellipsometric and contact-angle (CA) data for stepwise construction (increasing generations) of a coordination dendritic structure using "linear" molecule **2** and Zr^{4+} ions (Figure 2a, 2b) and similar construction using branched molecule **3** (Figure 2c, 2d), starting from dilute anchor SAMs (triangles in Figure 2). Dilute anchor SAMs were prepared by 16 h immersion of an improved OT SAM into a 0.1 mM ethanolic solution of **1**. The dendritic structures were obtained by alternate immersion of the substrate (with a dilute SAM of **1**) in solutions of Zr^{4+} ions and ligand **2** or **3**, [39] adding one generation in each step and always terminating with the organic ligand. For comparison, the same experiments were conducted on full anchor SAMs (circles in Figure 2).[39,43] The ellipsometric data are presented as changes in Δ (from bare gold) rather than as film thickness, to avoid ambiguity associated with the structure of the dendritic films.

Significant differences in growth mode on dilute SAMs of **1** are observed between the "linear" (**2**) and the branched (**3**) molecules (Figure 2, triangles). The ellipsometric −Δ values for **2** (Figure 2a, triangles) are nearly unchanged for the first two generations, followed by a moderate increase, and final overlap with the curve for a full anchor SAM after six generations. For **3**, the ellipsometric −Δ values increase after the first generation, coinciding with the curve for a full anchor SAM after four generations, generally showing a rather small deviation from the full layer (circles). The ellipsometric growth curves for the "linear" and branched molecules on dilute anchor layers intersect the growth curves obtained on full anchor SAMs at different generations, followed by complete overlap of the growth. The dilute anchor SAMs were prepared in an identical manner in both cases; therefore the significant differences suggest that the molecular structures of **2** and **3** play a major role in the growth pattern.

The CA values (Figure 2b, 2d) provide insight into the surface structure, due to the large wettability difference between the hydrophobic, methyl-terminated OT SAM and the hydrophilic, hydroxamate-terminated surface of **1**. The advancing CA for an improved OT SAM is 112° ± 0.4°, with a CA hysteresis[47] of 5°−10°.[45] Following 16 h of immersion in **1**, the advancing CA of the mixed SAM (denoted "generation 0") is 108° ± 2°, suggesting insertion of a minute amount of **1** into the OT SAM with nearly no change in the surface wettability. The CA values dramatically decrease for increasing dendrimer generations of both **2** and **3**, reaching steady low values coinciding with those obtained for layers grown on full anchor SAMs (ca. 40° for **2** and 20° for **3**). Similarly to the ellipsometry results, the CAs also show the difference between dendritic growth of **2** and **3**, where convergence of the CAs to the values measured on full anchor SAMs occurs at generation 4 for **2** and generation 2−3 for **3**. As the low CA values indicate domination of hydroxamate groups on the surface, the convergence following the construc-

(47) The CA hysteresis is defined as the difference between the advancing and receding CAs.

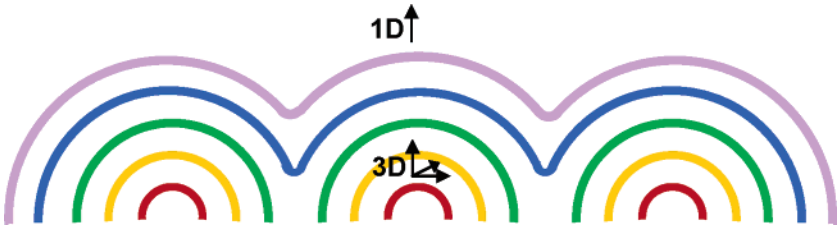

Figure 3. Schematic illustration of the growth of coordination dendritic structures from isolated anchor sites on the surface, emphasizing the transition from 3D to 1D growth which occurs upon dendrimer coalescence, and the efficient space-filling. Concentric semicircles indicate progressing generations.

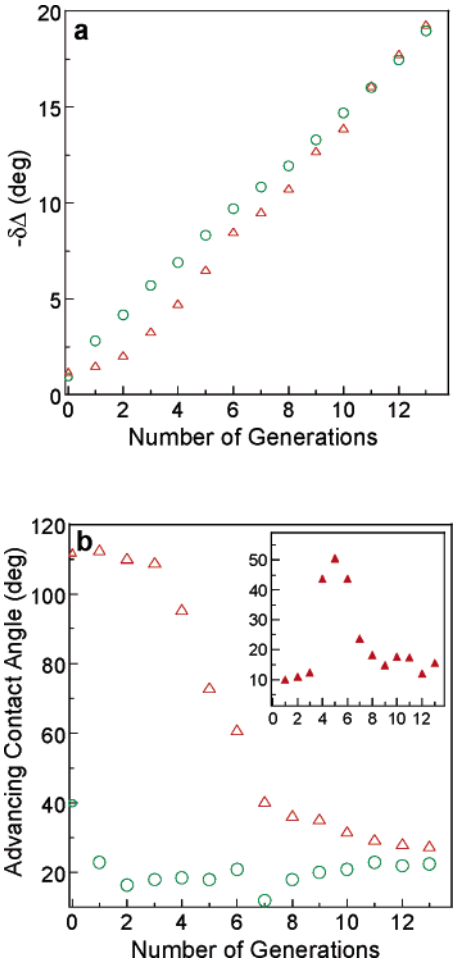

Figure 4. Changes in the ellipsometric Δ values (a) and advancing CAs (b) for the stepwise construction of 13 generations of the branched dendritic structure Zr^{4+}/**3** on highly dilute (triangles) and full (circles) layers of anchor **1** (the 0th generation represents the mixed OT + **1** SAM). Inset of b: CA hysteresis values (in degrees) for the construction on highly dilute SAM of **1**. Highly dilute OT + **1** SAMs were prepared by 100 min immersion of an improved OT SAM in 0.1 mM ethanolic solution of **1**.

tion of several generations manifests progress toward dendrimer overlap.

The combined results presented in Figure 2 are intuitively understood in terms of initial 3D growth of laterally spaced dendritic structures, followed by convergence and overlap of dendrimers with the growing number of generations, eventually obtaining full layers of **2** or **3** and regular 1D Layer-by-Layer (LbL) growth. The transition from 3D to 1D growth is much faster with the branched building block **3**, presenting excess hydroxamate groups and more efficient branching and lateral expansion.[39]

The results with ligand **2** are not readily understood. While branched ligand **3** bears three bishydroxamate groups, designed to accommodate nonlinear (dendritic) growth, such a growth mode is not expected for the "linear" (tetrahydroxamate) ligand **2**, where ion binding using the four hydroxamates as two bishydroxamate groups is not expected to leave extra hydroxamate groups for nonlinear growth. The initial nonlinear (dendritic) growth with ligand **2** is, therefore, likely to involve a certain fraction of monohydroxamate binding to Zr^{4+} ions, leaving free hydroxamate groups for branching, as previously suggested by us as an explanation for trans-metalation results in LbL growth of full layers of **2** and **3**.[39] The 3D growth and the transition to 1D growth are, however, more efficient with the branched ligand **3** (Figure 2), where the three bishydroxamate groups enable branching with full coordination, energetically more favorable than monohydroxamate binding. In both cases, we assume that an initial 3D film growth takes place (both lateral spreading and thickness increase) until the surface becomes predominantly hydroxamate-terminated, at which point the expansion reverts to normal 1D growth.

The fact that the ellipsometric curves for the dendritic structures perfectly coincide, after a number of generations, with the curves for films grown on full anchor SAMs (Figure 2a, c), is understood by considering the geometry of the system growth. As shown schematically in Figure 3, although the initial density of dendritic structures is low due to the spacing between anchor sites, the hemispherical growth geometry implies that when overlap is reached the gaps between the dendritic structures gradually close and the density approaches that of similar layers grown on full anchor SAMs.

The dilute anchor layers in the above experiments were prepared using relatively long immersion (16 h) of the OT SAM in a solution of **1**. The surface fraction (α) of anchor **1** can be roughly estimated from the changes in the CAs before and after immersion of the OT SAM in **1**, using the Cassie equation:[48]

$$\cos(\theta_M) = \alpha \cos(\theta_1) + (1 - \alpha) \cos(\theta_{OT})$$

where θ_M, θ_{OT}, θ_1 are the measured CA, the CA for a pure SAM of OT, and the CA for a pure SAM of **1**, respectively. Using $\theta_{OT} = 112° \pm 2°$,[45] $\theta_1 = 40° \pm 3°$,[39] a surface fraction $\alpha = 6 \pm 3\%$ is obtained, which is a relatively high fraction of **1** in the SAM. Such a high fraction is not suitable for actual observation of the growth of isolated dendrimers on the surface and the 3D-to-1D transition, for which highly spaced anchor sites are required.

A similar experiment was carried out using a much higher dilution of anchor **1**. Figure 4a (triangles) shows ellipsometric data for the assembly of a 13-generation dendritic structure of branched molecule **3** on a highly dilute anchor SAM, the latter prepared by much shorter immersion (100 min) of an improved

(48) Cassie, A. B. D. *Discussions of the Faraday Society* **1948**, *3*, 11−16.

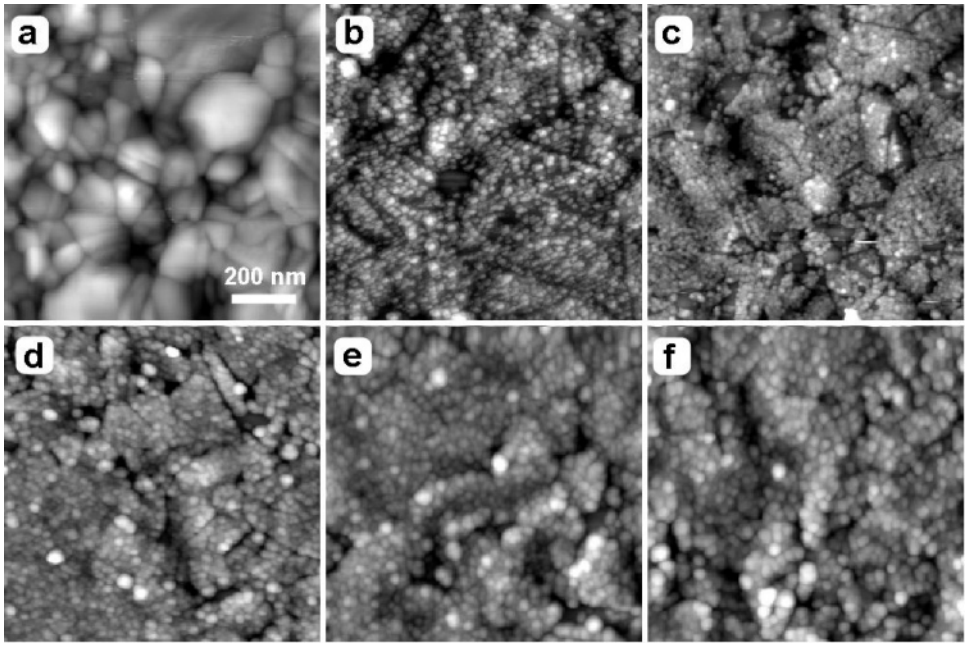

Figure 5. (a−f) Dynamic-mode AFM images of a highly dilute (as in Figure 4) OT + **1** SAM on gold substrate followed by 1, 3, 5, 9, 11, and 13 generations of the branched dendritic structure Zr^{4+}/**3**, respectively (z-scales for (a−f): 12, 13, 17, 20, 20, 17 nm, respectively). The scale bar in (a) applies to all images.

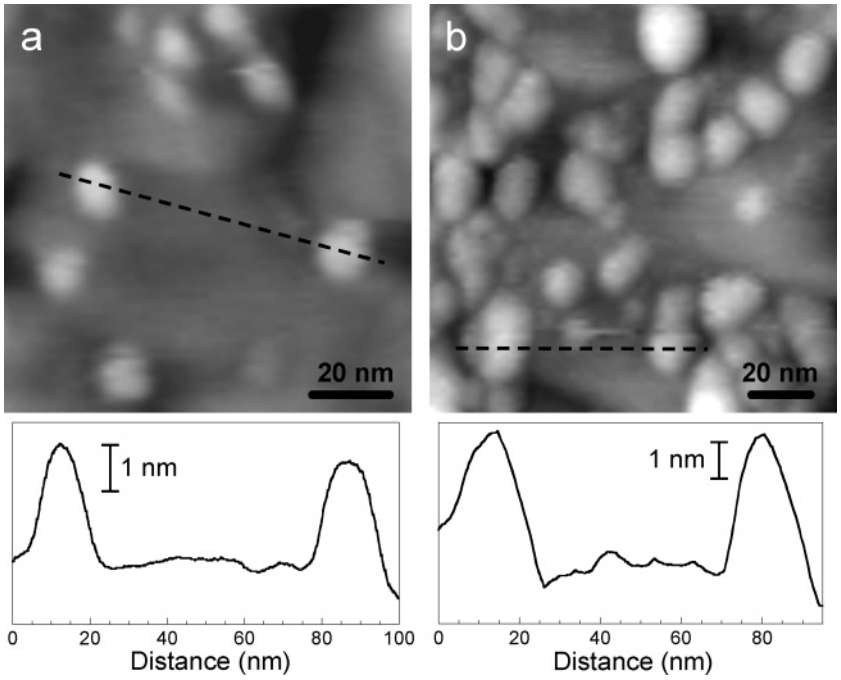

Figure 6. Dynamic-mode AFM images of isolated second (a) and third (b) generation Zr^{4+}/**3** dendrimers grown on a highly dilute OT + **1** SAM on gold. Line profiles through neighboring dendrimers (dashed lines in the images) are shown below the images. The heights of the dendrimers are 2.6 and 4.0 nm for the second and third generation, respectively.

OT SAM in a solution of anchor **1**. The results are also compared to those for a layer prepared similarly on a full anchor SAM (circles). The growth mode of the dendrimer in Figure 4a is qualitatively similar to that of the one grown on the less diluted anchor SAM (Figure 2c), but showing much larger deviations of the ellipsometric parameter Δ and delayed coincidence with the full layer, occurring at ca. 10th generation rather than 4th generation in Figure 2c. The results indicate that a considerably more dilute anchor layer is afforded by the shorter immersion in a solution of **1**, providing greater isolation of the growing dendritic structures.

The CA data shown in Figure 4b also support the above conclusions; the initial high CA values are extended to higher dendrimer generations, suggesting slow transformation of the predominantly methyl-terminated surface to a hydroxamate-terminated one. The CA hysteresis values (Figure 4b, inset) reach a maximum of 40°−50° at 4−6 generations. The hysteresis behavior generally follows the changes in the surface

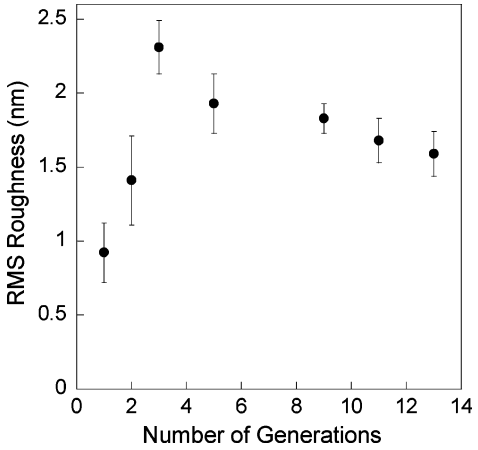

Figure 7. RMS roughness values for increasing generations of the branched dendritic structure Zr^{4+}/**3** grown on a highly dilute OT + **1** SAM on gold, calculated from the AFM images in Figure 5 (calculations performed on 200 × 200 nm^2 areas on individual gold grains).

roughness and heterogeneity,[49] both initially increasing as isolated dendritic structures emerge and grow, then decreasing as the structures begin to overlap.

Dynamic mode AFM images showing the development of 1, 3, 5, 9, 11, and 13 generations of Zr^{4+}/**3** dendrimers grown on a highly dilute anchor SAM (as in Figure 4) are shown in Figure 5a−f, respectively. The first generation (Figure 5a), comprising molecules of **3** protruding from the mixed OT + **1** SAM, shows no features on the surface at the given AFM resolution, except the well-known topography of the evaporated gold substrate, consisting of 100−400 nm {111}-textured crystalline grains. The third generation image (Figure 5b) reveals numerous scattered dendrimers covering the surface, superimposed on the surface topography of the gold substrate. The individual dendrimers are clearly resolved, somewhat varying in density in different regions. The latter is expected, given the fact that insertion of the anchor molecules is a random process, taking place mainly at defects in the OT SAM. The images in Figure 5c−f show further development and growth of the dendrimers, as well as increasing dendrimer overlap and coalescence, manifested as a gradual reduction in the density of features.

In early generations individual dendrimers can be resolved by the AFM and analyzed. Figure 6a, b shows, respectively, high-resolution AFM images of isolated second- and third-generation dendrimers. The height of the dendrimers, measured by the line profiles shown under the images, is 2.6 and 4.0 nm for the second and third generation, respectively. The apparent lateral dimensions of the dendrimers are similar in both images (10−20 nm), evidently reflecting tip convolution rather than dendrimer lateral projection.

The best estimate for the number of dendrimers per unit surface area (dendrimer density) is obtained from AFM images of third generation dendrimers (Figure 5b), where the dendrimers are developed enough to be easily imaged but still relatively far apart to minimize underestimation due to tip convolution. The apparent dendrimer density in Figure 5b is high, but this visual impression is misleading due to tip-size related effects. In contrast, the water CA for the third generation dendrimers is 109° (Figure 4b), indicating a very low fractional coverage by the dendrimers.

(49) See ref 38, p 54.

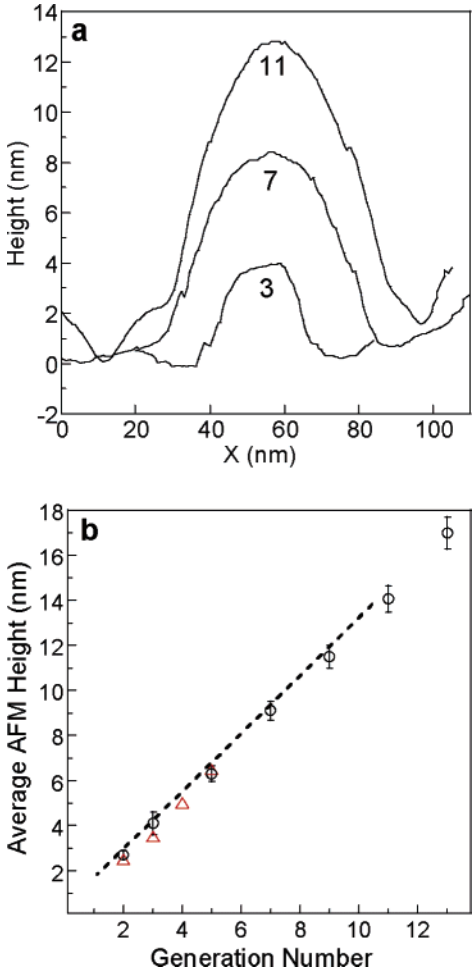

Figure 8. (a) AFM line section profiles of laterally isolated Zr^{4+}/**3** dendrimers on highly dilute OT + **1** SAMs on gold (generation numbers are indicated). (b) Circles: Average AFM heights of different generations of the dendritic structures (obtained by measuring the height of isolated features or voids). Triangles: Height values of 2−5 generation dendrimers, from theoretical molecular models (Figure 9). Dashed line: Best-fit height curve for multilayers of **3** on a full SAM of **1** (from Figure 6c in ref 39).

To estimate the dendrimer density, the protruding features in Figure 5b were counted in the image. The resulting density obtained by counting separate 200 × 200 nm^2 areas is 1800 ± 200 dendrimers/μm^2, which translates to an average center-to-center spacing of 24 ± 3 nm. Assuming that each dendrimer grows from a single molecule of **1** on the surface (a lower-limit assumption), the initial fraction of **1** in the mixed SAM would be ca. 0.05%. This minute fraction, attesting to the extremely high dilution of anchor **1**, is below the detection limits of common surface analysis techniques. Dendrimer growth therefore functions as a sensitive "developing reagent" for the surface composition, as previously shown by coordination binding of gold nanoparticles functionalized with ligand **1**.[45]

The RMS surface roughness in the AFM images (Figure 5) was analyzed for different generations, and the results are presented in Figure 7. As discussed above in the context of the CA hysteresis, the general shape of the roughness curve is consistent with the initial roughness increase as dendrimers begin to develop, followed by a gradual decrease associated with dendrimer overlap and coalescence. The sharp increase in the roughness in the first three generations is followed by a gradual decrease to a value of ~1.6 nm at generation 13, a value which

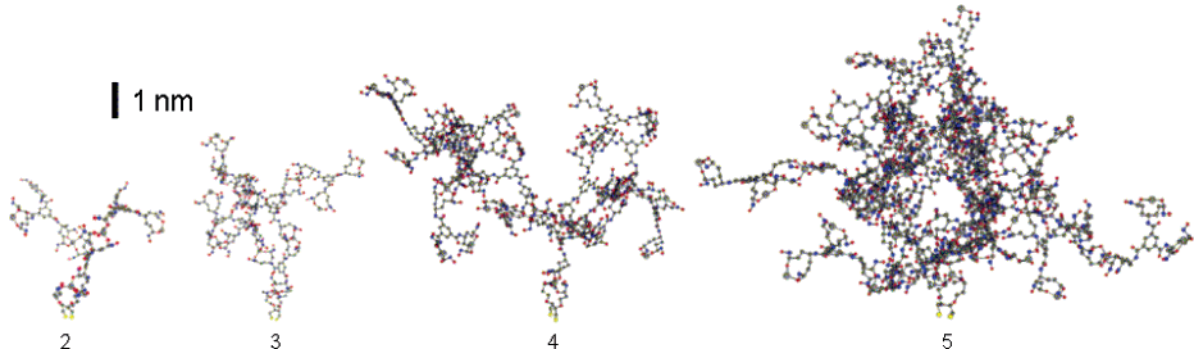

Figure 9. Energy-minimized molecular models of 2−5 generations of Zr^{4+}/**3** bound to anchor **1** (anchor **1** is shown at the bottom in all models).

is higher than that for multilayers grown on a full anchor SAM (∼0.5 nm).[39] It is therefore concluded that at increasing generation numbers the surface dendrimers coalesce and form a continuous film whose average thickness at generation 13 is similar to that of a film grown on a full anchor SAM (Figure 4a), but the thickness uniformity is lower and still improves with added generations.

It is interesting to compare the CA hysteresis values, showing a maximum at 5 generations (Figure 4b, inset), to the AFM roughness analysis, with a maximum at 3 generations (Figure 7). The discrepancy may be attributed to two factors: (i) The CA hysteresis is influenced by both surface roughness and heterogeneity, i.e., the increasing hydrophilic character of the surface with added generations. (ii) Tip convolution, i.e., the AFM tip is not capable of resolving dendrimers larger than third generation, which is why the measured roughness is highest at that point.

The height of dendrimers of the different generations was measured by line profiles in the AFM images, choosing regions where isolated structures can be imaged (at higher generations, such spots are difficult to find). Figure 8a shows representative line profiles of 3, 7, and 11 generation dendrimers, while the heights of all dendrimer generations are summarized in Figure 8b. The solid line in the figure corresponds to the height of multilayers of **3** grown on a full SAM of **1**[39] (subtracting the height of a SAM of **1**). The dendrimer heights are remarkably identical to the heights of the regular multilayers of **3**, supporting the growth mode depicted in Figure 3. This, together with the consistent coincidence of the ellipsometric curves for higher generations in Figures 2 and 4, implies that the growth of the dendritic structures on dilute anchor surfaces proceeds with exceedingly efficient filling of voids (Figure 3). The latter suggests the possibility of generating high-quality films, essentially irrespective of the anchor density in the first layer down to 0.05%.

Energy-minimized models of 2−5 generations of Zr^{4+}/**3** dendrimers grown on a molecule of **1** are shown in Figure 9.[50] The 3D shape of the dendrimers is not hemispherical but rather odd-shaped (the modeled 2D projections (not shown) are roughly spherical). The distance between two bishydroxamate groups in each molecule of **3** is roughly 1.5 nm, as seen most clearly in the second generation model. With increasing generation number the dendrimers become more globular and assume a more dense structure. Using the models, the estimated vertical protruding dimensions of the dendrimers (not including the height of **1**, which, in the real case, is embedded in an OT SAM) are 2.5, 3.5, 5, and 6.5 nm for generations 2−5, respectively. These values are marked in Figure 8b and are in excellent agreement with the experimentally measured height values.

(50) MM2 energy minimized models were calculated using CS ChemDraw and CS ChemBats3D software, Cambridgesoft, USA.

Table 1. XPS Atomic Concentration % at Different Takeoff Angles for a 13-Generation Dendritic Film Grown from a Highly Dilute Anchor SAM on Gold, as in Figure 5f[a]

takeoff angle	C	O	N	Zr	S	Au
35°	58.5	26.1	12.9	1.8	0.2	0.8
45°	57.2	26.9	13.0	1.8		1.1
90°	55.7	27.1	13.1	1.8	0.4	1.6
90° [b]	56.6	26.7	11.3	2.9	0.9	1.4

[a] For comparison, the last row shows XPS data for a 10-layer multilayer of **3** grown on a full SAM of **1**. [b] Constructed on a full anchor SAM (from Table 1 in ref 39).

To verify the basic scheme of dendritic growth via coordination binding to anchor **1** in the SAM, blank experiments were carried out (published elsewhere)[45] using **1**-functionalized gold nanoparticles (NPs). Briefly, pure OT SAMs exposed to Zr^{4+} followed by the modified NPs did not show any NP binding, while OT + **1** SAMs subjected to the same treatment showed NP binding which depended on the amount of **1** in the layer, as visualized by AFM. These experiments confirmed that binding occurs through metal-ion coordination to the surface anchors.

The composition of a 13-generation dendritic film of Zr^{4+}/**3** was analyzed by angle-resolved XPS, and the results are summarized in Table 1. The data show nearly no dependence of the dendritic layer elements on the takeoff angle, implying that the atoms are evenly distributed in the layer, as previously reported for coordinated multilayers constructed similarly on full anchor layers.[39] The chemical composition is nearly identical in the two cases, i.e., a 13-layer dendritic film and a 10-layer multilayer, the latter shown in the last row of Table 1. A significant exception is the N/Zr concentration ratio, which is 4:1 in the multilayer and 7.3:1 in the dendritic film. In a fully non-cross-linked multilayer the theoretical N/Zr ratio is 4.5:1,[39] whereas in a totally cross-linked structure, such as a perfect dendrimer, the ratio is 6:1. The corresponding experimental N/Zr values are in qualitative agreement with the theoretical values, indicating, as expected, more extensive cross-linking in the dendritic film. The deviations from the theoretical values suggest some excess, noncoordinated Zr^{4+} in the multilayers[39,43] and a certain fraction of free hydroxamate groups in the dendritic film.

Conclusions

Highly controlled divergent growth of coordination dendrimers on surfaces was demonstrated. Both "linear" (tetrahydrox-

amate) and branched (hexahydroxamate) molecular building blocks, formally providing two and three ion-binding groups, respectively, afford dendritic growth on highly dilute anchor monolayers on gold. The branched ligands exhibit more efficient divergent growth, attributed to the excess available hydroxamate groups. Growth of coordination dendrimers from laterally isolated anchor ligands starts with 3D growth and evolution of laterally spaced dendrimers, which, at higher generations, leads to coalescence and a 1D growth mode similar to that of ordinary multilayers grown on full anchor SAMs. Isolated dendrimers were imaged by AFM, and their dimensions (i.e., height) match those obtained from molecular models as well as the thicknesses of the ordinary multilayers. The combined ellipsometric and AFM data indicate that the 3D-to-1D growth of coordinated dendritic structures progresses via a highly efficient continuous space-filling process. Our approach to the divergent generation of surface dendrimers is relatively simple, does not require complex synthesis, and yields surfaces decorated with dendrimers of controlled dimensions. The size control achieved using this method allows nanometer-scale tuning of surface properties by properly adjusting the number of steps. The present scheme provides excellent dendrimer size control and statistical lateral distribution; the latter can be improved by using different patterning approaches. Further, the developed method enables functionalization of the dendrimer surface by binding functional peripheral ligands, as well as introduction of functionalities to the branched ligands, thus achieving amplified properties (e.g., optical, catalytic, analytic, and others) via dendritic growth. The LbL approach points to the possibility of multiple derivatization, by using different ligands and functional groups in different generations.

Acknowledgment. I.R. and A.V. acknowledge support from the Israel Science Foundation, Grant No. 307/03, and the Minerva Foundation, with funding from the Federal German Ministry for Education and Research. M.W. was partially supported by a Levy Eshkol Scholarship, Israel Ministry of Science. We thank Dr. H. Cohen (Weizmann Institute) for the XPS measurements.

JA061761Q